Indian Journal of Chemical Technology
Vol. 24, January 2017, pp. 32-39

Low-temperature synthesis of Cr_2WO_6 and its enhanced photocatalytic activity by N-doping

K Sravan Kumar, G Ravi, Sreenu K, Ravinder Guje & M Vithal*
Department of Chemistry, University College of Science, Osmania University, Hyderabad 500 007, India
E-mail: mugavithal@gmail.com

Received 25 July 2015; accepted 16 June 2016

Nano sized inverse trirutiles of composition Cr_2WO_6 and N-doped Cr_2WO_6 have been prepared by sol-gel and solid state methods respectively. Urea has been used as a source of nitrogen for N-doping. These trirutiles have been characterized by powder X-ray diffraction (PXRD), FT-IR, TGA, scanning electron microscopy (SEM), energy dispersive spectra (EDS), and UV-visible diffuse reflectance spectroscopy (UV-vis DRS). N-doped Cr_2WO_6 is crystallized in the tetragonal lattice with space group $P4_2/mnm$ (136). The bandgap energy of both parent and N-doped materials is deduced from their UV-visible DRS profiles. The photocatalytic degradation of methylene blue and methyl violet aqueous solutions have been investigated using these oxides. Compared to the parent material, nitrogen doped Cr_2WO_6 exhibits ~ 30% and ~ 20 % increase in visible light-induced photo-degradation of the methylene blue (MB) and methyl violet (MV), respectively.

Keywords: Nitrogen doping, Photodegradation, Powder X-ray diffraction, Sol-gel method

Research on photocatalytic technology continue to attract the scientific and industrial community due to its possible applications in harvesting the solar energy. It is widely acknowledged that semiconductor mediated photocatalysis has the potentiality to address the environmental problems like water and air cleaning as well as to generate hydrogen by water splitting[1-5]. The water pollution due to the release of organic pollutants (dyes) from textile industries is a pertinent issue and demands novel green photocatalytic routes leading to the alternative materials to TiO_2. Titanium dioxide (TiO_2) with a bandgap of 3.2 eV is considered as a bench mark material and has been extensively studied due to its remarkable properties such as high stability, low cost and non-toxicity. However, its utility in visible light is limited due to its wide bandgap energy. Therefore, a diversity of photocatalysts with band edge positions which allow visible absorption will be required to deal with different pollutants under visible light conditions of the existing semiconducting materials, oxides have received considerable attention as the photocatalyst for water splitting and degradation of organic pollutants[6-10].

The general formula of ternary oxides belonging to the trirutile family is $A^{2+}B_2{}^{5+}O_6$. The structure of trirutile can be considered as a super structure of rutile ($A^{4+}O_2$) with a regular distribution of the A^{2+} and B^{5+} ions in the tripled rutile cell (Fig. 1). The A^{2+} and B^{5+} cations are surrounded by O^{2-}octahedra. Goldschmidt was the first to report trirutile-type structure for the minerals tapiolite ($FeTa_2O_6$) and mossite ($FeNb_2O_6$)[11]. Subsequently, several trirutile (AB_2O_6) structure type oxides have been reported, where A^{2+} is V, Cr, Mg, Co, Cu and Fe, and $B^{5+}$is Nb, Sb and Ta[12-16]. The trirutile structure is stable as long as the radii of the A and B ions are similar and about ~0.6 to 0.75 Å. It crystallizes in the tetragonal lattice with space group $P4_2/mnm$. The Wyckoff positions for A and B are *2a* (0, 0, 0) and *4e* (0, 0, *z*) respectively. In the inverse trirutile-type structure, positions for A and B cations are interchanged (i.e., The Wyckoff positions for A and B are *4e* (0, 0, *z*) and *2a* (0, 0, 0)) respectively and the composition becomes A_2BO_6 (Fig. 1)[17,18].

Cr_2WO_6 is a ternary oxide belonging to the inverse trirutile family of formula $A_2{}^{3+}B^{6+}O_6$. It was first synthesized by Bayer via solid state method. Based on the X-ray diffraction data, Bayer found that oxide with the composition of $A_2{}^{3+}B^{6+}O_6$ (where A = $A1^{3+}$, Cr^{3+}, Ga^{3+}, or Fe^{3+} and B = W^{6+}, Te^{6+} and Mo^{6+}) has inverse trirutile type structure. Although the structure and thermodynamic properties of Cr_2WO_6 have been studied, its photocatalytic properties are not reported to our knowledge[18,19]. The present investigation is aimed at studying the photocatalytic properties of parent and nitrogen (N) doped Cr_2WO_6. The nitrogen

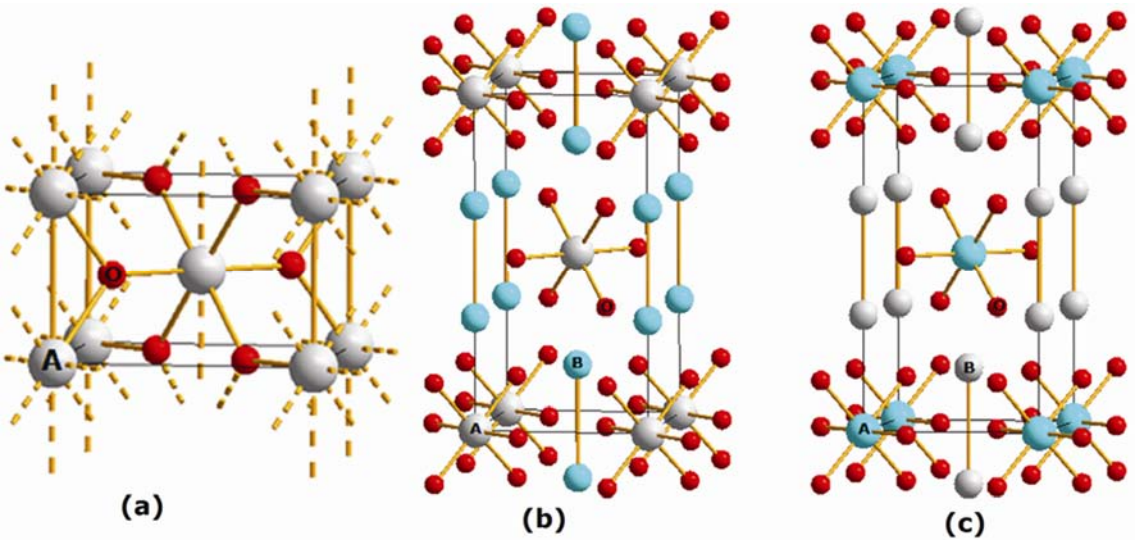

Fig. 1 — The structures of (a) Rutile, (b) Trirutile and (c) Inverse trirutile

was doped into the Cr_2WO_6 with the idea of tailoring its photocatalytic and optical properties. In general, improved photocatalytic activity for N-doped oxides is due to the dopant-induced modulation of the electronic structure through the mixing of N 2p orbitals with O 2p orbitals within the valence bands (VB), shifting band-to-band threshold excitation energies to longer wavelengths[20]. In N-doped oxide materials, the holes generated from N 2p by visible light excitation, are active species for decomposition of organic pollutants, although the efficiency of charge separation under visible excitation is lower than that under UV excitation[21,22]. In the present work an attempt is made to prepare Cr_2WO_6 by soft chemical route and investigate its visible light photocatalytic activity against methylene blue and methyl violet dyes.

Experimental Section

Preparation of Cr_2WO_6 (CWO)

G Bayer has prepared Cr_2WO_6 by heating the stoichiometric quantities of Cr_2O_3 and WO_3 in air at 600, 700, 800, 900, 1000 and 1100°C for 20 h. each in an oxidizing atmosphere[17]. We have adopted sol-gel citrate method for the preparation of this compound. A stoichiometric amount of $Cr(NO_3)_3$ $9H_2O$ was first dissolved in double distilled water and labeled as "solution A". Tungsten metal powder was dissolved in H_2O_2 solution in an ice bath. It takes about 6 h for complete dissolution of tungsten powder. The resultant clear solution was labeled as "solution B". Solution A was slowly added to solution B. The chelating agent, citric acid, was added. The molar ratio of citric acid to metal ions was 2:1. The *p*H of the resultant metal citrate solution was adjusted to 6-7 by adding dilute ammonia solution drop wise. The solution was then slowly evaporated on a water bath till a viscous liquid was obtained. At this stage, the gelating reagent, ethylene glycol was added to the solution. The molar ratio of citric acid to ethylene glycol was 1.0:1.2. This mixture was heated on a hot plate at 100°C for 2-3 h with constant stirring. The temperature was increased to 160-180°C at the onset of solidification. The ensuing solid porous mass was ground in an agate mortar using spectral grade acetone. The resultant black powder was heated in a muffle furnace at 500-900°C for 6 h each in the steps of 100°C.

Preparation of N-doped Cr_2WO_6 (CWON)

The N-doped CWO ($Cr_2WO_{6-x}N_y$) was obtained by heating a well ground mixture of CWO and urea at 400°C for 2 h in a muffle furnace. The weight ratio of CWO to urea was 1:2. The resultant powder was washed several times with deionized water to remove excess unreacted urea and byproducts.

Characterization

The powder X-ray diffractograms were recorded on Rigakuminiflex 600 powder X-ray diffractometer at room temperature in the 2θ range 10–80° for phase confirmation using Cu Kα radiation of wavelength 1.5406 Å. The step size and scan step time were 0.02° and 0.15 s, respectively. Infrared spectra were recorded in the form of KBr pellets in the wave number range 4000–400 cm^{-1} using JASCO IR-5300 spectrometer. Thermogravimetric analysis (TGA) was

performed using Shimadzu differential thermal analyzer (DTG-60H) with a heating rate of 15 °C min^{-1}. The SEM-EDS images were recorded on the HITACHI SU-1500 variable pressure scanning electron microscope (VP-SEM). JASCO V-650 UV-vis spectrophotometer was used for UV-vis diffuse reflectance spectra (DRS) measurements in the range 200-900 nm. $BaSO_4$ was used as the reflectance standard.

Photocatalytic activity measurement

The photoactivity of these samples was studied by photodegradation of methylene blue (MB) and methyl violet (MV) under visible light irradiation employing a 300 watts W lamp ($380 < \lambda < 840$ nm) in HEBER visible annular type photoreactor. In a typical process, the catalyst (50 mg) was added to an aqueous solution of MB / MV (1×10^{-5} M) in a cylindrical-shaped glass reactor at room temperature in air. The suspension was stirred in the dark for 60 min to establish adsorption - desorption equilibrium before visible light irradiation. During irradiation, at regular time intervals of 30 min, about 3-5 mL of the solution was collected, centrifuged to remove the catalyst particles and analyzed by JASCO V650 UV-vis spectrophotometer. The degraded amount of MB / MV is reported as $d = \frac{(C_0 - C)}{C_0}$ where 'C' is the concentration of MB / MV at each irradiated time, and 'C_0' is the concentration of MB / MV at equilibrium.

Results and Discussion

Powder XRD

Parent Cr_2WO_6 and N-doped Cr_2WO_6 are prepared by sol-gel and solid state methods respectively. Tungsten metal powder was used for the first time as W source instead of WO_3 in the preparation of Cr_2WO_6. The precursor of CWO is calcined at 500, 600, 700, 800 and 900°C separately for 6 h each. The room temperature powder XRD patterns of CWO sintered at above mentioned temperatures are shown in Fig. 2. The samples heated below 500°C gave broad background without any diffraction features indicating the amorphous nature of the sample. The diffraction lines were observed for the sample sintered at or above 500°C. Thus, the crystallization temperature of CWO is around 500°C. The XRD patterns of these samples are similar with reported CWO data [JCPDF-73-2236] and free from impurities. The structural analysis of CWO was carried out using

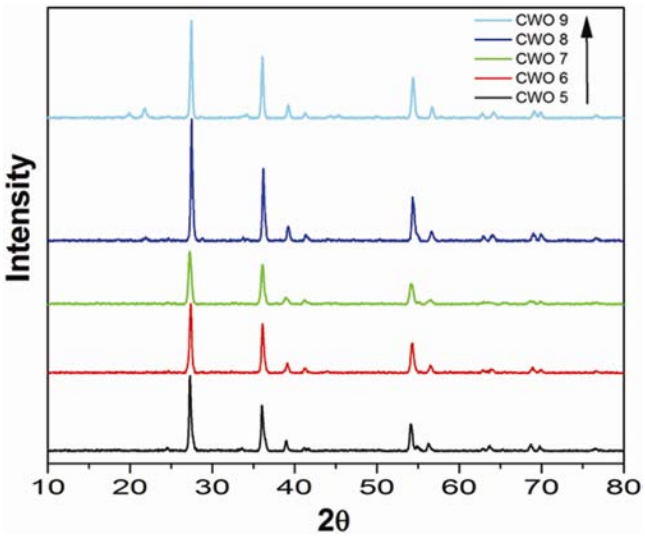

Fig. 2 — Powder XRD patterns of CWO at 500°C (CWO5), 600°C (CWO6), 700°C (CWO7), 800°C (CWO8) and 900°C(CWO9)

the Rietveld refinement program, Fullprof.2k (Version 5.30). The following methodology was followed while refining the XRD data of CWO. The program begins with the correct space group, reasonably good starting lattice parameters, atomic coordinates within the unit cell and estimated occupation number. Firstly, scale factor and background parameters were fitted. The diffraction peak profile was fitted with a pseudo-Voigt profile function. The *x* and *z* parameters of oxygen (*4f* and *8j* sites) were refined. It is noticed from the Rietveld refinement that CWO was found to crystallize in the tetragonal lattice with space group $P4_2/mnm$ (136). The obtained lattice parameters*a (=b) and c* of CWO were found to be 4.589 and 8.878 Å, respectively. These values are very close to reported unit cell parameters[18]. The experimental and theoretical powder diffraction profiles for CWO, are shown in Fig. 3. The atomic positions, including fractional coordinates of the oxygen are given in Table 1.

The powder pattern of CWON is similar to that of CWO. Nevertheless, when powder pattern of CWON was plotted in an expanded scale, the diffraction peaks show a shift towards lower 2θ value indicating a change in unit cell parameters and the substitution of nitrogen into the CWO lattice. The d-lines of CWON were least square fitted using POWD software to obtain the unit cell parameters. It is found that CWON also crystallized in the tetragonal lattice with space group $P4_2/mnm$ (136) and the obtained unit cell length values, *a (=b) and c*, are 4.584 and 8.887 Å, respectively. Thus, CWON also crystallizes

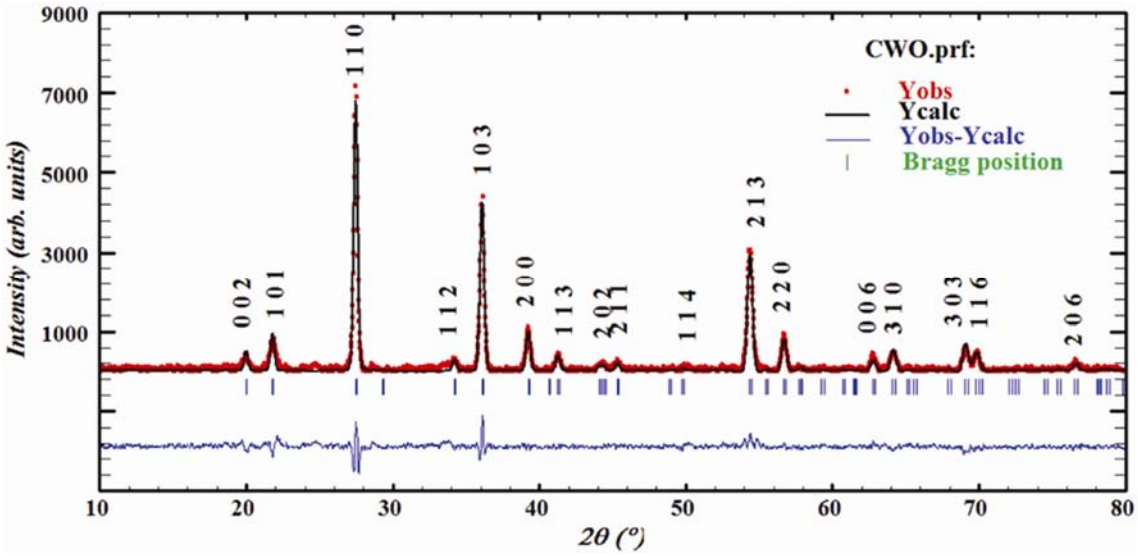

Fig. 3 — Observed, calculated and difference XRD pattern profiles of CWO, prepared at 900°C

Table 1 — The atomic positions of Cr_2WO_6 structure, including fractional coordinates of the oxygen.

Atom	Wyckoff position	Atomic coordinates		
		x	*y*	*z*
Cr	*4e*	0	0	0.333
W	*2a*	0	0	0
O1	*4f*	0.299	0.299	0
O2	*8j*	0.297	0.297	0.35027

in trirutile structure with the regular distribution of the CrO_6 and WO_6 octahedra and partial substitution of oxygen by nitrogen. The observed marginal changes in unit cell lengths are due to the partial substitution of nitrogen into CWO lattice. As the ionic radius of N^{3-} (0.171 nm) is higher than that of O^{2-} (0.140 nm), partial replacement of O by N should increase the unit cell parameter. The observed and calculated d-values for the CWON along with *hkl* values are given in Table 2. The crystallite size of CWO and CWON was calculated from the line width of the intense diffraction line (110) using the Scherer's formula[23]

$$t = \frac{0.9\lambda}{\beta \cos\theta}$$

where t is the thickness in angstrom (Å) and corresponds to the crystallite diameter assuming a spherical shape, λ is the wave length of the X-ray used, θ is the Bragg angle and β is the full width at half maximum measured in radians of intense line in the powder XRD pattern. The crystallite sizes of the CWO and CWON were found to be 35 nm and 34 nm respectively.

Table 2 — The observed and calculated d-values for the CWON along with *hkl* values

hkl	CWON	
	d_{obs}	d_{cal}
002	4.4554	4.4424
101	4.0923	4.0744
110	3.2478	3.2420
112	2.6170	2.6188
103	2.4901	2.4877
200	2.2923	2.2925
113	2.1887	2.1866
202	2.0392	2.0372
211	2.0081	1.9979
114	1.8251	1.8324
213	1.6850	1.6858
220	1.6222	1.6210
006	1.4882	1.4808
310	1.4483	1.4499
303	1.3591	1.3581
116	1.3468	1.3469
206	1.2431	1.2439

FT-IR spectra

The IR spectra of trirutiles, CWO and CWON, were recorded to find out the presence of water and nitrogen in the lattice. The FTIR spectra of CWO and CWON in the range 250-4000 cm^{-1}. The FTIR spectrum of CWO exhibits bands at 367, 468, 553, 613, and 704 cm^{-1}, which are characteristic vibrational bands of trirutile structure[24]. The IR spectrum of CWON differs from that of CWO in two ways. First, the band positions have been shifted to lower

wavenumbers. Second, new bands in the region 1000-1500 cm^{-1} (at 1249, 1328, and 1413 cm^{-1}) have appeared. These new bands can be attributed to the presence of nitrite and hyponitrite groups on the surface of CWON[25]. These two differences confirm the N doping into the CWO lattice. Further, when W-O (Cr-O) bonds are replaced by W-N (Cr-N), the bond length increases (due to a higher ionic radius of N^{3-}) leading to a decrease in the force constant. Lower force constant results in a lower stretching or bending vibrational frequency. The observed shift in the band positions is in agreement with this argument[26]. The weak and broad band observed for CWON around 3500 cm^{-1} indicates the presence of water in the lattice. This is further confirmed by thermogravimetric analysis (TGA).The intensity of this band in CWO is almost insignificant.

Thermogravimetric analysis (TGA)

Thermogravimetric (TG) curve of the nitrogen doped CWON is characterized by two weight loss regions. The weight loss in the temperature region 30-250°C is 0.05%. This weight loss can be ascribed to adsorbed water on the CWON. The weight loss of 0.11% observed in the region 250-600°C can be attributed to the decomposition of chemisorbed unstable species.

SEM-EDS

The morphology of the CWO and CWON was studied by scanning electron microscope (SEM) (Fig. 4). The SEM image of both CWO and CWON show non-spherical shaped irregular size micro crystallites with considerable agglomeration. The presence of N1s peak in EDS of CWON also confirms the N-doping into CWO. An estimation of nitrogen content in CWON was also obtained from EDS measurements (Fig. 4). From the EDS data, the nitrogen content (in wt. %) for CWON was found to be 0.62.

Diffuse reflectance spectra analysis

The light absorption properties of the CWO and CWON are investigated. The absorption spectra (DRS) of these materials in the range 200-900 nm.

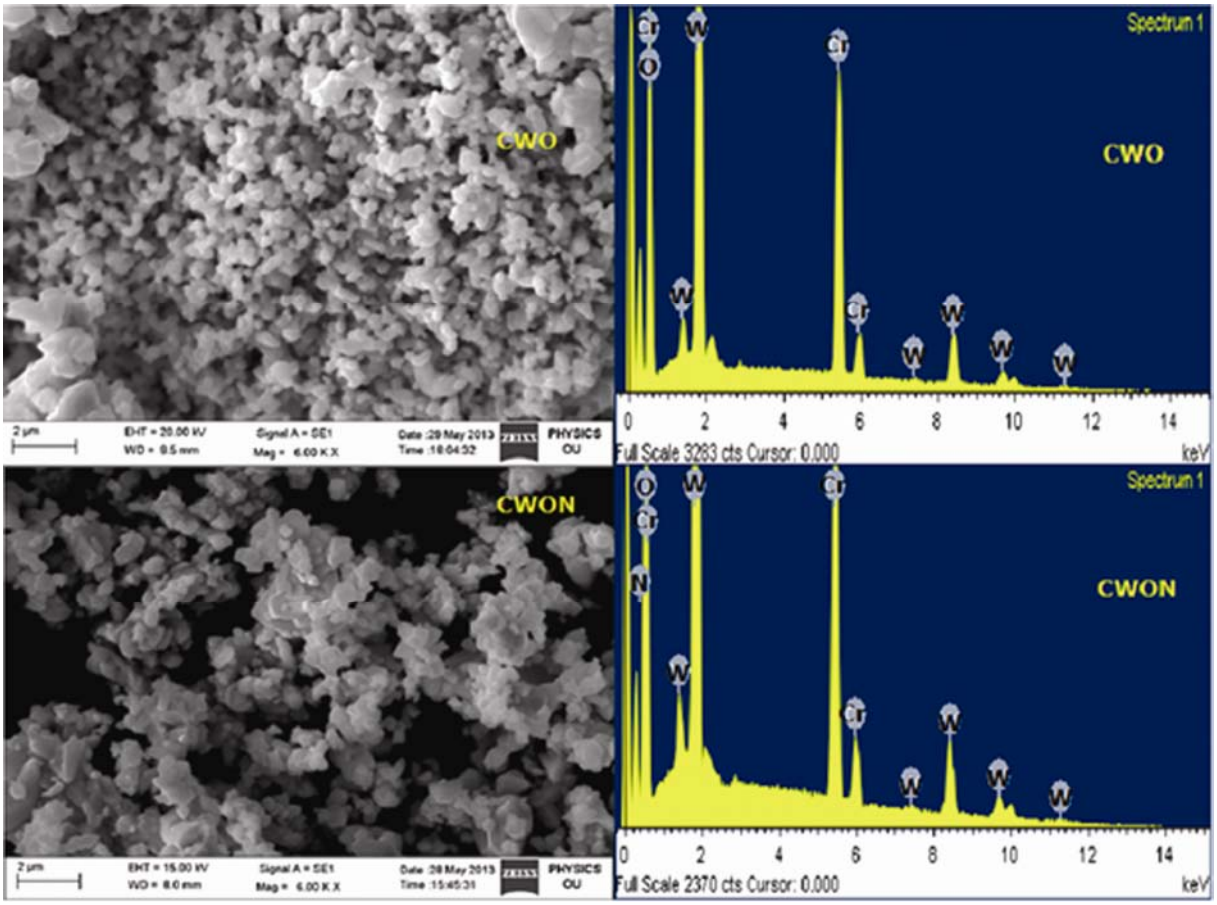

Fig. 4 — SEM-EDS images of CWO and CWON

The spectra were characterized by peaks belonging to Cr^{3+} in the visible region and steeply increasing profile in the lower wavelength region. Trivalent chromium ($3d^3$) with a ground state of $^4A_2$ (F) in octahedral coordination is expected to give three spins allowed transitions (a, b, c) and a spin forbidden transition (d) as shown below[27]:

$$^4A_{2g}(F) \rightarrow {}^4T_{2g}(F) \quad \text{... (a)}$$

$$^4A_{2g}(F) \rightarrow {}^4T_{1g}(F) \quad \text{... (b)}$$

$$^4A_{2g}(F) \rightarrow {}^4T_{1g}(P) \quad \text{... (c)}$$

$$^4A_2 \rightarrow {}^2E \quad \text{... (d)}$$

The optical spectra of CWO and CWON are characterized by a broad envelope in the 350-600 nm range, a less broad peak at 700-800 nm and a charge transfer band at 250-300 nm. In the present investigation, the transitions (a) and (b) are merged in the wavelength region 350-600 nm and the transition (c),*i.e.* $^4A_{2g}(F) \rightarrow {}^4T_{1g}(P)$ is overlapped with the charge transfer transition. The less broad band centered at ≈745 nm corresponds to transition (d). The absorption band edge of the samples was obtained by extrapolating the horizontal and sharply rising part of the curves onto the wavelength axis. The edge of each absorption peak was shifted towards longer wavelength side for CWON indicating the change in the band structure due to the substitution of nitrogen into CWO lattice. The band gap energy of semiconducting oxides can be obtained from the Kubelka-Munk plot of $(Kh\nu)^{1/2}$ vs. hν. Extrapolation of the linear part of the plot to $(Kh\nu)^{1/2} = 0$ (i.e. on to the x-axis) provides an estimation of the band gap energy. Figure 5 shows the Kubelka-Munk (KM = $(Kh\nu)^{1/2}$) plot for both CWO and CWON samples and the estimated band gap for these samples is found to be 1.82 and 1.67 eV respectively. Thus, the introduction of nitrogen into the CWO lattice reduces the band gap energy as observed from the red shifts of the absorption band edge. It can be ascribed to the widening of the valence band, resulting from the hybridization of N 2p and O 2p orbitals[28].

Photodegradation of methylene blue (MB) and Methyl violet (MV)

The photocatalytic activity of CWO and CWON is evaluated by degradation of MB and MV under the visible light irradiation. Figure 6 shows the temporal

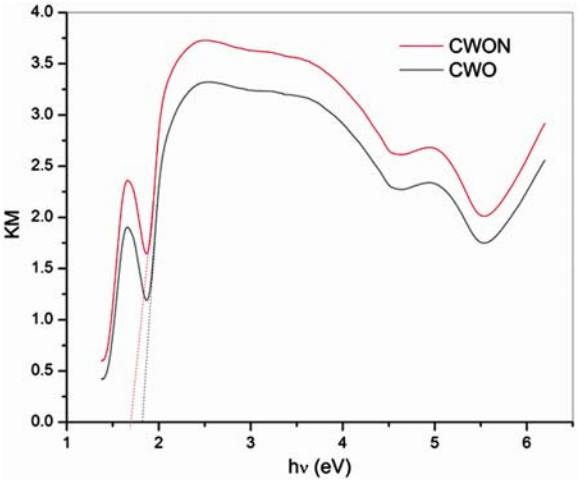

Fig. 5 — KM plot of CWO and CWON

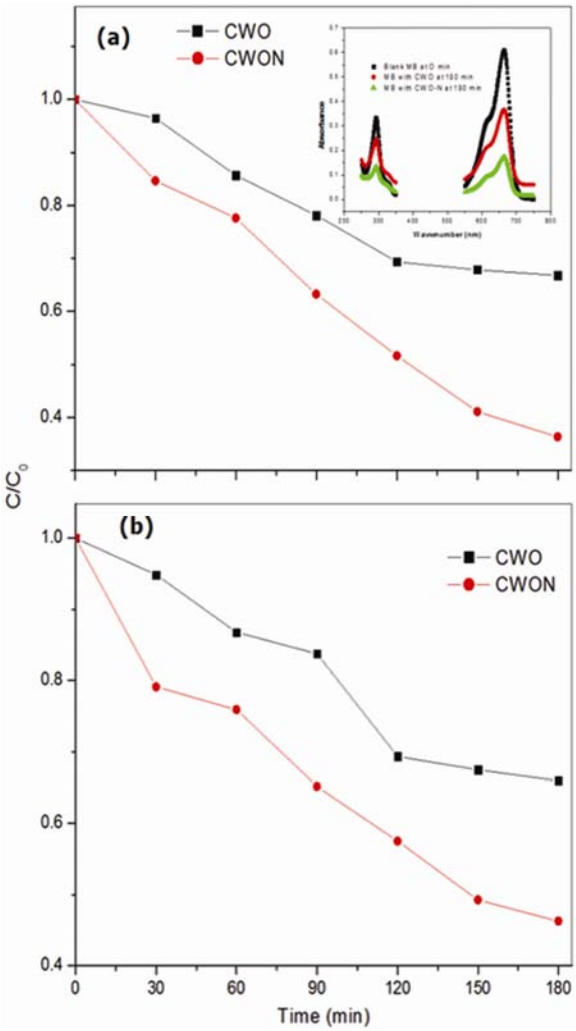

Fig. 6 — Temporal changes in (a) MB and (b) MV concentration in the presence of CWO and CWON under visible light irradiation. The inset shows the MB absorption spectra at different time intervals of irradiation

changes in the concentration of aforementioned organic dyes in the presence of CWO and CWON. The degradation of MB/MV was measured by following the variations in maximal absorption in their UV-visible spectra at 664/580 nm. Before the irradiation experiments, the samples were kept in the dark chamber for attaining the adsorption-desorption equilibrium. Under the light irradiation, it is noticed that the degradation of MB/MV increased with an increase in the irradiation time (Fig. 6). Fig. 6a (inset) shows the UV-visible spectra of MB at different time intervals of irradiation. The absorption spectrum of MB is characterized by a medium band at ~300 nm and a strong band at ~675 nm with a shoulder at ~600 nm. The band at ~300 nm is attributed to the aromatic ring, whereas the overlapping bands at ~600 and ~675 are assigned to conjugated π – system. The decrease in absorbance of MB with increasing irradiation time indicates that both the materials in the present study have exhibited photoactivity against MB degradation under visible light irradiation. The extent of MB degradation after 180 min of irradiation seen for the CWO and CWON is 41 and 72%, respectively. Figure 6b shows the variation in MV concentration with irradiation time in the presence of CWO and CWON. After 180 min of irradiation, the degradation of MV in the presence of CWO and CWON was 34% and 54%, respectively. A comparison of the photoactivity of CWO and CWON shows the following features: (a) the photoactivity of CWO against MB and MV degradation is negligible beyond the 120 min of visible light irradiation (b) the rate of degradation in the presence of CWON is higher compared to that of CWO and (c) CWON exhibits ~30% and ~20% increase in visible light-induced photo-degradation of the methylene blue (MB) and methyl violet (MV), respectively.

The photocatalytic activity of a material depends on several factors such as surface area, the degree of crystallinity, bandgap energy and structure of the material. The physical processes, including light absorption, the transport of charge carriers and the recombination rate of photogenerated electron-hole pairs are persuading the photocatalytic efficiency of a photocatalyst. In this study, the enhanced photoactivity for N-doped CWO may be attributed to (a) decrease in the bandgap energy of CWON resulting in an increase in the number of absorbed photons and (b) defects created in the lattice due to the incorporation of nitrogen leading to a reduction in the electron-hole recombination rate. Similarly, the low rate of degradation of MV compared to MB in the presence of CWON may be depends on its molecular structure, extent of ionization in aqueous solution, and adsorbing capacity of the catalyst[29].

Table 3 — The kinetic parameters (k, $t_{1/2}$) and correlation coefficient (R^2) for CWO and CWON

Photocatalyst (Dye)	First order rateconstant, k, min^{-1}	Square of correlation coefficient R^2	$t_{1/2}$ (min^{-1})
CWO (MB)	0.00253±0.00026	0.95	274
CWON (MB)	0.00582±0.00027	0.99	119
CWO (MV)	0.00257±0.00026	0.95	270
CWON (MV)	0.00422±0.00026	0.98	165

Kinetic study to predict the rate constant for the degradation reactions

The kinetics of MB and MV degradation in the presence of both the catalysts was also studied. The degradation reaction of MB / MV with CWO and CWON shows pseudo first order kinetics (Langmuir-Hinshelwood model)[30]. The results were nearly consistent with linear equation

$$\ln\left(C/C_o\right) = -kt$$

For the pseudo first order reaction, the half-life time ($t_{1/2}$) can be calculated according to the equation

$$t_1/2 = \frac{ln2}{k}$$

A linear correlation (R^2), suggest that the degradation reaction follow the first-order kinetics. The slope of the linear line gives the first order rate constant. The kinetic parameters (k, $t_{1/2}$) for both photocatalysts are given in Table 3.

Conclusion

Cr_2WO_6 is prepared for the first time by sol-gel method. Nitrogen doped Cr_2WO_6 is prepared by a facile solid state reaction method using urea as a source of nitrogen. Powder XRD patterns confirm its phase formation. CWON is crystallized in the tetragonal lattice. Based on the EDS profile, the nitrogen content in CWON was found to be 0.62 Wt %. The incorporation of nitrogen into CWO lattice is confirmed from (a) shift in the d lines of powder patterns (b) the presence of N peak in its EDS profile and (c) shift in the absorption edge in UV-visible DRS profiles. The bandgap energy of N doped CWO is reduced by about 0.15 eV. The nitrogen doped CWO has shown higher photoactivity against the

methylene blue and methyl violet degradation under visible light irradiation. Compared to the parent material, CWON exhibits ~30% and ~20% increase in visible light-induced photo-degradation of the methylene blue (MB) and methyl violet (MV), respectively. The MB and MV degradation in the presence of CWO and CWON follow pseudo first order kinetics.

Acknowledgements

The authors gratefully acknowledge the Department of Science & Technology (DST), New Delhi under FIST and University Grants Commission (UGC), New Delhi under UPE-FAR schemes for financial assistance. One of the authors, G. Ravi thanks, University Grants Commission (UGC), New Delhi for the assistantship under UGC-BSR RFSMS scheme.

References

1 Ochiai T, Hayashi Y, Ito M, Nakata K, Murakami T, Morito Y & Fujishima A, *Chem Eng J*, 209 (2012) 313.
2 Ismail A A & Bahnemann D W, *Sol Energy Mater Sol Cells*, 128 (2014) 85.
3 Zong X & Wang L, *J Photochem Photobiol C: Photochem Rev*, 18 (2014) 32.
4 Cho H S, Gokon N, Kodama T, Kang Y H & Lee H J, *Int J Hydrogen Energy*, 40 (2015) 114.
5 Helali S, Polo-López M I, Fernández-Ibáñez P, Ohtani B, Amano F, Malato S & Guillard C, *J PhotochemPhotobiol A: Chem*, 276 (2014) 31.
6 Marschall R & Wang L, *Catal Today*, 225 (2014) 111.
7 Du W, Zhu Z, Zhang X, Wang D, Liu D, Qian X & Du J, *Mater Res Bull*, 48 (2013) 3735.
8 Pu Y, Li Y, HuangY, Kim S I, Cai P & Seo H J, *Mater Lett*, 141 (2015) 73.
9 Sales H B, Bouquet V, Députier S, Ollivier S, Gouttefangeas F, Guilloux-Viry M, Dorcet V, Weber I T, de Souza A G & Garcia dos Santos I M, *Solid State Sci*, 28 (2014) 67.
10 Ravi G, Suresh P, Veldurthi N K, Reddy J R, Hari Padmasri A & Vithal M, *Int J Hydrogen Energy*, 39 (2014) 15352.
11 Goldschmidt V M, Barth T, Holmsen D, Lunde G & Zachariassn W, *Skr Norske Vidensk-Akad Oslo, Mat-Naturvidensk KI*, 1 (1926).
12 Lee H J, Kim I T & Hong K S, *Jpn J Appl Phys*, 36 (1997) L1318.
13 Weitzel H & Klein S, *Acta Crystallogr A*, 30 (1974) 380.
14 Reimers J N, Greedan J E, Stager C V & Kremer R, *J Solid State Chem*, 83 (1989) 20.
15 Ramos E, Fernández F, Jerez A, Pico C, Rodríguez-Carvajal J, Saez-Puche R & Veiga M L, *Mat Res Bull*, 27 (1992) 1041.
16 Nakua A, Greedan J E, Reimers J N, Yun H & Stager C V, *J Solid State Chem*, 91 (1991) 105.
17 Bayer G, *J Am Ceram Soc (Discussions and Notes)*, 43 (1960) 495.
18 KunnmannW, La Placa S, Corliss L M & Hastings J M, *J Phys Chem Solids*, 29 (1968) 1359.
19 Jacob K T, *J Mater Sci*, 15 (1980) 2167.
20 Asahi R, Morikawa T, Ohwaki T, Aoki K & Taga Y, *Science*, 293 (2001) 269.
21 Katoh R, Furube A, Yamanaka K & Morikawa T, *J Phys Chem Lett*, 1 (2010) 3261.
22 Tang J, Cowan A, Durrant J & Klug D, *J Phys Chem C*, 115 (2011) 3143.
23 Vogel A I, *Textbook of Quantitative Chemical Analysis* (Longman Group Ltd, Harlow, U. K.) 1989.
24 Clark G M & Doyle W P, *Spectrochim Acta*, 22 (1966) 1441.
25 Sakthivel S, Janczarek M & Kisch H, *J Phys Chem B*, 108 (2004) 19384.
26 Yang N, Li G, Yang X, Wang W & Zhang W F, *Dalton Trans*, 40 (2011) 3459.
27 Ravi G, Veldurthi N K, Muvva D P, Munirathnam N R, Prasad G & Vithal M, *J Nano Part Res*, 15 (2013) 1939.
28 Sun C, Mukherji A, Liu G, Wang L & Smith S C,*Chem Phys Lett*, 501 (2011) 427.
29 Ravi G, Veldurthi N K, Palla S, Velchuri R, Pola S & Vithal M, *Photochem Photobiol*, 89 (2013) 824.
30 Talebian N & Nilforoushan M R, *Thin Solid Films*, 518 (2012) 2210.